nature communications

Article

https://doi.org/10.1038/s41467-025-59689-z

Optical control of RKKY coupling and perpendicular magnetic anisotropy in a synthetic antiferromagnet

Received: 9 January 2024

Accepted: 30 April 2025

Published online: 12 May 2025

Check for updates

Meiyang Ma[1,2], Jing Wu[3,4] ✉, Bo Liu[1,2] ✉, Lei Wang[5], Zhuoyi Li[1,2], Xuezhong Ruan[1,2], Zehua Hu[2], Fengqiu Wang[2], Xianyang Lu[1,6], Tianyu Liu[7], Jun Du[7], Ke Xia[5] & Yongbing Xu[1,2,4,6] ✉

Synthetic antiferromagnetics (SAF) provide an excellent platform for antiferromagnetic spintronics. Recently, the voltage-control of the Ruderman–Kittel–Kasuya–Yosida (RKKY) interaction in SAFs was studied experimentally. Optical control would offer unique opportunities for the ultrafast manipulation of spin states, however, it has yet to be demonstrated. Here, using femtosecond laser excitations in a [Co/Pt]-based perpendicular magnetic anisotropy (PMA) synthetic antiferromagnet (p-SAF), we drive a reduction of the RKKY coupling and the PMA. We attribute the reduced RKKY interaction to the optically smeared Fermi wave vector of the Ru layer, which mediates the exchange coupling between the constituent ferromagnetic layers. The PMA exhibits the same amplitude of decrease as the RKKY coupling, which we associate with electron redistributions in the 3*d* orbitals caused by the optically smeared Fermi level. While the pump excitation process is shown to have an influence on the modulations, thermal contributions are excluded. Our study establishes a link between the RKKY coupling and the PMA in a p-SAF structure and provides an approach to tune them in parallel.

Antiferromagnetic (AF) spintronics has emerged as a major field in spintronics, fueled by its remarkable attributes of high magnetic field (H-field) stability and ultrafast operation speed[1–7]. However, this robustness also leads to a weak response to an external magnetic fields, which hampers conventional magnetic control methods[8,9]. Synthetic AF materials (SAF), however, offer great opportunities for AF devices due to their relatively weak exchange coupling. SAFs typically consist of two ferromagnetic (FM) layers separated by a metallic or an insulating spacer, where two FM layers are magnetically coupled via Ruderman-Kittel-Kasuya-Yosida (RKKY)-type exchange interaction mediated by nonlocal spin-polarized carriers of the space layer[10]. In an SAF structure, ferromagnetic or antiferromagnetic coupling can be controlled via the thickness and material of the nonmagnetic space layer[11].

Control of the exchange coupling in SAFs shows promise for facilitating fast and efficient magnetization switching in devices. Recent experiments have demonstrated that an electric field can tailor the RKKY coupling and drive transitions between AF and FM[12–14]. These effective modulations typically rely on changes of the Fermi level influenced by charge accumulations at the surface or ion doping by applying a voltage[15–18]. Because of efficient charge screening in metallic SAF structures, charge accumulation by the E-field is usually limited to the outmost surface/interface and therefore indirectly affects the RKKY coupling arising from the FM/NM interface. Ion migration into

[1]National Key Laboratory of Spintronics, Nanjing University, Suzhou, China. [2]School of Electronic Science and Engineering, Nanjing University, Nanjing, China. [3]School of Integrated Circuits, Guangdong University of Technology, Guangzhou, China. [4]School of Physics, Electronics and Technology, University of York, York, UK. [5]Key Laboratory of Quantum Materials and Devices of Ministry of Education, School of Physics, Southeast University, Nanjing, China. [6]School of Integrated Circuits, Nanjing University, Suzhou, China. [7]Department of Physics, Nanjing University, Nanjing, China. ✉e-mail: jing.wu@york.ac.uk; boliu@nju.edu.cn; ybxu@nju.edu.cn

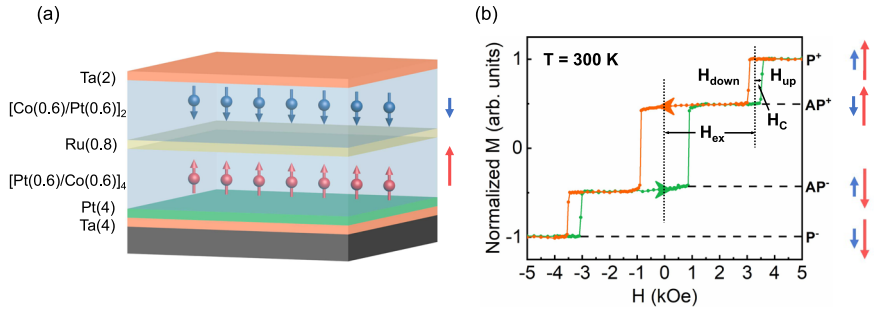

Fig. 1 | SAF-sample structure and the static magnetic properties. a SAF sample schematics. **b** Static out-of-plane hysteresis loop measured by VSM. The green and orange lines represent the process that sweeps the magnetic field from negative to positive and from positive to negative, respectively. The switching fields of the minor loop in two sweeping branches are defined as H_{up} and H_{down}, respectively. The RKKY coupling field H_{ex} and the coercivity H_C are extracted from H_{up} and H_{down}.

the SAF driven by E-field may somehow cause additional chemical or structural complexity[19]. Optical control of the RKKY coupling is therefore preferable for its advantages of simpler fabrication, inner-interface access[20,21] and flexibility[22].

Optical manipulation of the RKKY interaction was initially investigated in semiconductor quantum dot systems and II-VI diluted magnetic semiconductors[23–25], where the exchange interaction can be established by virtual electron-hole pairs or excitons generated by a sub-band-gap optical excitation[26]. However, equivalent modulation of the RKKY interaction in an SAF has not been performed yet. Manipulating the interlayer coupling by femtosecond laser pulses is key for ultrafast spin dynamics such as all-optical switching (AOS) where the RKKY coupling is reported to mediate magnetization switching as little as a few picoseconds[27,28].

Meanwhile, the interfacial magnetic anisotropy constant is an important parameter in a perpendicular SAF structure. We note that although E-field control of magnetic anisotropy energy (MAE) has been studied in ferromagnets[29,30], the systematic consideration of MAE variations during the E-field control of the RKKY coupling, for example in synthetic antiferromagnets, has not been explored, yet it is essential in both fundamental and technical aspects. As they both show interfacial origins, we expect there would be a connection between the manipulation of the MAE and the RKKY coupling.

Here, we use antiferromagnetically coupled $[Pt/Co]_4$/Ru/$[Co/Pt]_2$ as a prototype system to investigate optical manipulations of the RKKY interaction and the interfacial PMA. We show by time-resolved magneto-optical Kerr effect (TR-MOKE) that a fs laser pulse can simultaneously and equally tune the RKKY coupling and the PMA in the $[Pt/Co]_4$/Ru/$[Co/Pt]_2$ system. Upon pump excitations the RKKY strength and the coercivity of a ferromagnetic layer are scaled to the same extent. The modulated RKKY and coercivity shows no dependence on pump-probe delays, excluding contributions of the magnetization amplitude as it varies as a function of the pump-probe delays. This suggests that the optical modulations originate from the Ru space layer which dominates the RKKY exchange coupling. We propose that the pump laser excites conduction electrons of the nonmagnetic Ru layer into a trapped states (e.g., defects or impurities) at the interface leading to a reduction of Fermi wave vector k_F of the Ru conduction layer, and therefore minimizing the RKKY coupling between two FM layers. The shift in the Fermi level (E_F) associated with this change in the k_F alters the electron occupation at the Pt/Co interface and thus the perpendicular coercivity of the constituent FM layer. Our results provide insights into how a femtosecond laser pulse modulates the RKKY interaction and PMA, thereby enabling control of magnetization switching processes in a SAF system for applications in ultrafast magnetic data storage.

Results

Figure 1a illustrates the layer structure of the composite film used in our experiment. The SAF stack consists of Ta(4)/Pt(4)/$[Pt(0.6)/Co(0.6)]_4$/Ru (0.8)/$[Co(0.6)/Pt(0.6)]_2$/Ta(2) (thicknesses in nanometers). The 2 nm Ta capping layer is used to prevent sample oxidation. Here, the unit of $[Pt(0.6)/Co(0.6)]_4$ is read as the bottom ferromagnetic layer, and the $[Co(0.6)/Pt(0.6)]_2$ is set as the top ferromagnetic layer. Figure 1b shows an out-of-plane hysteresis loop measured by a vibrating sample magnetometer (VSM). The top and bottom ferromagnetic layers are antiferromagnetically coupled. The SAF system can be manipulated into four distinct magnetization states of P^+, AP^+, AP^- and P^- by an external magnetic field. The blue and red arrows denote the magnetization directions of the top and bottom multilayers, respectively. The bottom $[Pt/Co]_4$ layer is magnetically hard, while the top $[Co/Pt]_2$ layer is magnetically soft (Supplementary Note 1). The antiferromagnetic coupling field H_{ex} can be obtained from the minor loop shift of the top layer. In Fig. 1b, H_{up} and H_{down} in the minor hysteresis loop indicates the switching field in the up and down sweeping directions of the external field, respectively. The minor loop displays a substantial net positive shift of 3.29 kOe (referred to as the antiferromagnetic coupling field H_{ex}) obtained via $(H_{up} + H_{down})/2$. H_{ex} is proportional to the RKKY exchange coupling. Meanwhile, the coercivity of the $[Co/Pt]_2$ soft layer can be represented as $H_C = (H_{up} - H_{down})/2$, showing a magnitude of 0.24 kOe.

Figure 2a displays transient minor hysteresis loops measured at the time delay where the largest demagnetization amplitude is reached for different pump fluences. The minor loop is measured in a field range where the magnetically hard bottom layer is magnetically fixed after an initial positive saturation of the whole system. At a low pump fluence of $F = 0.96$ mJ/cm^2, the switching fields H_{up} and H_{down} are comparable to their counterparts in the case of without pump pulses. At higher pump fluences of $F = 3.20$ mJ/cm^2 and 5.60 mJ/cm^2, H_{up} shows a noticeable decrease while H_{down} remains unchanged. To quantitatively analyze the effect of pump fluence on minor loops, we plotted in Fig. 2b H_{ex} and H_C as a function of pump fluence. H_{ex} decreases from 3.16 kOe to 3.02 kOe, while H_C displays a decline from 0.23 kOe to 0.07 kOe. They approximately show the same reduction of magnitude, namely $\Delta H_{ex} \approx \Delta H_C = 0.16$ kOe. This suggests an intrinsic coherence of the optical modulations on H_{ex} and H_C by increasing the pump fluence. Similar results in a series of samples with different RKKY strength by changing the Ru thickness and the [Co/Pt] repetition number are observed (Supplementary Note 2), confirming the reliability and the consistency of our results.

We notice that the H_{ex} and the H_C show similar and weak dependence on the pump-probe delays. Figure 2c displays "snapshots" of the transient minor hysteresis loops the time delays of $\Delta t = 0.063$ ps, 0.630 ps, and 9.763 ps (Supplementary Note 3 determines the time zero by fitting the demagnetization curve). The pump fluence is fixed at $F = 5.60$ mJ/cm^2. The amplitude of the transient minor hysteresis loops corresponds to the pump-induced demagnetization amplitude. It is notably diminished at $\Delta t = 9.763$ ps, indicating a substantial recovery of the magnetic order. Within the observed time window of

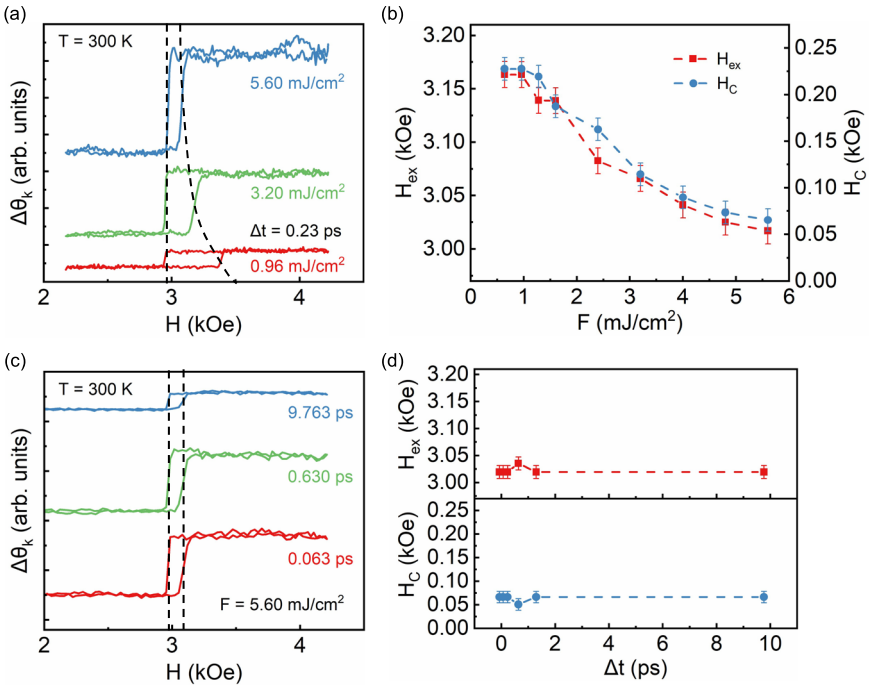

Fig. 2 | TR-MOKE measurements. a Transient minor hysteresis loops at selected pump fluences. As guided by the dashed lines, H_{up} shows an obvious reduction at high pump fluences while H_{down} remains unchanged. **b** Calculated H_{ex} and H_C values from the minor loops as a function of pump fluence F. Within experimental error bars they show the same trend after fs excitations. **c** Minor hysteresis loops probed at three different pump-probe delays under a fixed pump fluence of 5.60 mJ/cm². **d** Extracted time-delayed H_{ex} and H_C from transient loops in (**c**), showing negligible variations within 10 ps. Error bars indicate the uncertainty in determining the displayed value from the experimentally measured data.

the demagnetization process (~10 ps), the extracted H_{ex} and H_C show no pump-probe dependence except at Δt = 0.63 ps as shown in Fig. 2d whose y-axis ranges (~0.2 kOe) are the same as those of Fig. 2b. The amplitudes of the small spikes at Δt = 0.63 ps in Fig. 2d are much smaller than ΔH_{ex} and ΔH_C. The transient magnetization as shown in Fig. S4b drops first and then recovers within a few ps. Meanwhile, the extracted H_{ex} and H_C at different time delays as included in Fig. 2d remain stable. This suggests that the changes of H_{ex} and H_C by a fs light pulse are not correlated with transient magnetization amplitude.

It has been demonstrated that a fs laser pulse can excite the domain nucleation and the domain wall propagation due to circular dichroism[31], which may contribute to the variations of magnetization switching behavior. By changing circular polarization of pump beam, we have found that both the H_C and H_{ex} in our system show no dependence on circular polarization of the pump beam as detailed in Fig. S10a, b. This indicates that the possible light-induced domain wall propagation does not take effects here.

We have further considered whether thermal effects could lead to the concomitant reductions of H_{ex} and H_C. The thermal heating is an unavoidable factor when the pump fluence is increased. We recorded the minor loops as a function of the temperature by both the SQUID in Fig. 3a, b and the MOKE measurements in Fig. 3c, d. In Fig. 3a, as the temperature T increases from 300 K to 380 K, H_{up} and H_{down} decreases simultaneously and the minor loop shifts towards the negative-field direction. It is revealed that H_{ex} shows a reduction of ~ 0.4 kOe from 3.22 kOe at 300 K to 2.82 kOe at 380 K. In parallel, H_C shows only a marginal fluctuation of ~ 0.05 kOe. We further confirm this behavior ($\Delta H_{ex} > \Delta H_C$) through MOKE measurements by changing the static temperature. The employed pump fluence is fixed at F = 2.40 mJ/cm². As shown in Fig. 3d, H_{ex} decreases by 0.4 kOe while H_C stays constant at ~0.08 kOe for a temperature increase of 80 K. The SQUID results can exclude possible contributions of the inhomogeneous weights of the individual layer due to the optical penetration depth or multilayer reflections in the MOKE.

As shown in Fig. 3b, d by increasing the static temperature, H_{ex} varies even for a temperature increase of 20 K. This suggests that H_{ex} shows very sensitive dependence on thermal effect. According to the three-temperature model, transient lattice temperature typically increases to an equilibrium at a few ps after fs excitations[32,33]. However, the extracted time-delayed H_{ex} and H_C in Fig. 2d do not change up to 10 ps, indicating that within this timescale there is no noticeable transient temperature rise. In addition, the TR-reflectivity ΔR/R (Fig. S9 in Supplementary Note 9) shows a negative dip within 1 ps, indicating that non-thermal electrons are scattered before they couple to the lattice system. If thermal heating plays a role, the ΔR/R signal should show a growing positive component, which represents the lattice temperature, by increasing pump fluence as reported by Shim et al.[34]. However, the normalized ΔR/R in Fig. S9 are all negative with no fluence dependence. It has been shown in a multilayer structure that transient electron temperature decays rapidly to the ambient temperature within 1 ps before it couples to its lattice temperature[35]. Therefore, it can be concluded that any possible thermal effects do not play a major role for the concomitant variations of H_{ex} and H_C upon fs excitations.

Discussion

As discussed above, the nonchanged H_{ex} at various pump-probe delays suggests that upon fs excitations the magnetization magnitude has a minor impact on the RKKY interaction. The RKKY interaction can be described by the following effective Hamiltonian[36]

$$H = -\sum_{i,j} J\left(R_{ij}\right) S_i \cdot S_j \tag{1}$$

where $R_{ij} = R_i - R_j$; S_i is the spin operator on the atom i and $J\left(R_{ij}\right)$ is the exchange interaction between the neighboring spins on sites i and

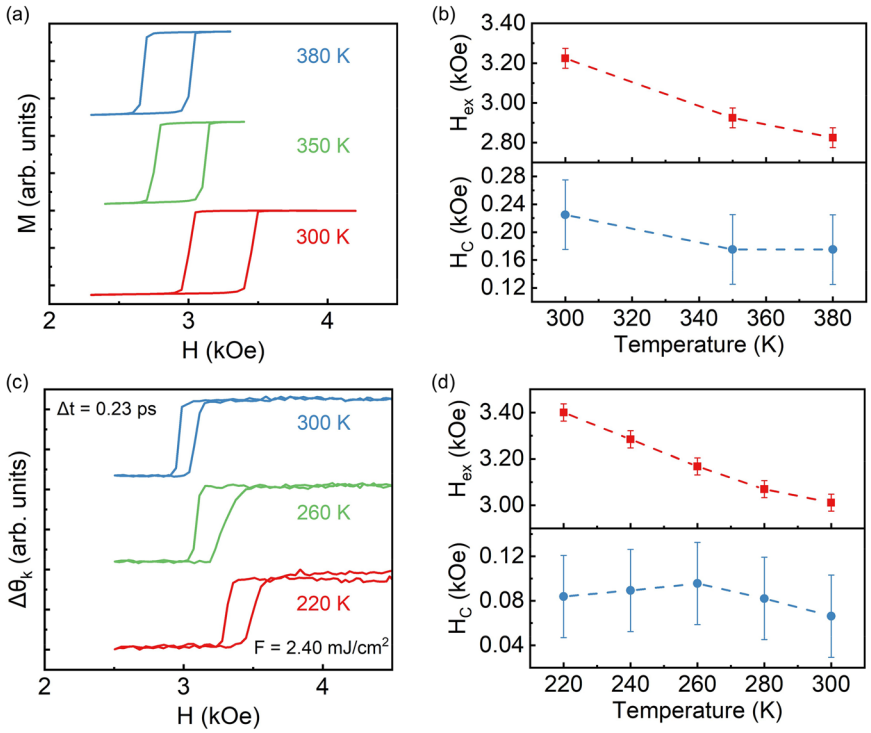

Fig. 3 | Temperature-dependent minor hysteresis loops. a Temperature-dependent minor hysteresis loops by SQUID. Both H_{up} and H_{down} are changed with the static temperature. **b** Extracted H_{ex} and H_C from (**a**) as a function of temperature. H_{ex} decreases with the increase of the static temperature while H_C stays unchanged within experimental error bars. **c** Temperature-dependent minor hysteresis loops by MOKE at a fixed pump fluence F of 2.40 mJ/cm^2. As in (**a**), similar shifts of H_{up} and H_{down} are shown. **d** Extracted H_{ex} and H_C from (**c**). The complementary magneto-optical method again confirms that a temperature increase of 80 K only affects H_{ex}, but not H_C. Error bars indicate the uncertainty in determining the displayed value from the experimentally measured data.

j. This guides us to relate the RKKY reductions to the modulation of $J\left(R_{ij}\right)$ by the fs laser pulses.

In a metallic multilayer sample, when two magnetic thin films (referred to as S_1 and S_2) are separated by a non-magnetic spacer layer with a thickness of d, the interlayer exchange coupling constant per unit area at the interface can be defined as J_{12}. This constant oscillates in both the sign and the magnitude within the spacer layer and decays as $1/z^2$, where z represents the distance from a selected reference layer within the thin films. In the limit of a large distance z, J_{12} takes on a simple form[36]:

$$J_{12}(z) = J_0 \frac{d^2}{z^2} sin(2k_F z) \tag{2}$$

where J_0 is a constant, and k_F represents the Fermi wave vector. In our experimental setup, the thickness d of the spacer layer remains constant. Therefore, the principal focus must be on the variations of the Fermi wave vector k_F by fs laser pulses, which can affect the RKKY interaction as well as shown by Eq. 2.

We accordingly propose a diagram in Fig. 4a to explain the simultaneous reductions of the RKKY interaction and the PMA by fs laser pulse excitations. When the sample is irradiated with a fs laser pulse, it can introduce nonequilibrium electron distributions at the Co/Ru interface. When trapping states (such as defects or impurities) exist above the Fermi level E_F, photoexcited holes near the E_F will cause a downward shift of the E_F, thus leading to a new E_F'. These trapping states allow much longer lifetimes of the photoholes than the 10 ps timescale that we have observed. As shown in Fig. S9, the initial negative ΔR/R dip indicates absorptions of photoexcited electrons/carriers, showing the existence of trapping states. The drop in photocarriers consequently introduces a deformation potential, a manifestation of carrier-density change. This launches a picosecond strain wave pulse[37,38], which can drive coherent phonon oscillations.

The oscillation period lasts for ~75 ps, suggesting that trapping states remain stable within such a few tens of ps. This is consistent with the fact that H_C and H_{ex} do not change as a function of time delays within 10 ps. By increasing pump fluence, H_C and H_{ex} change clearly, in accordance with the fact that the trapping states can be more filled upon larger pump fluence.

The Ru space layer is a nonmagnetic metal, whose conduction electrons can be described by the free-electron dispersion model of $E = \left(\frac{hk}{2m}\right)^2$ Consequently, as depicted in the right-lower part Fig. 4a, the decrease of E_F proportionally leads to a reduction in the Fermi wave vector k_F, and thus to a decrease of the RKKY interaction (or equivalently the H_{ex}). The photocarrier lifetime of hundreds of picoseconds have also been observed in other magnetic heterostructures[39].

Using the lattice structure in Fig. 5a, the light manipulation of the AF coupling can be understood by the first-principle calculations using a Green function method with TB-LMTO[40] (Supplementary Note 4). Electron transitions in metals by a laser can result in a corresponding decrease in the Fermi energy[22,41]. We can qualitatively reveal the light-manipulated AF coupling as a function of the Fermi energy. The calculated AF coupling (J_{ex}) versus Fermi energy shift ($E - E_F$) is shown in Fig. 5b. It can be observed that as the Fermi energy decreases, the AF coupling continues to decrease. The theoretical calculations are consistent with the above proposed model.

In 3d ferromagnetic metal/noble metal, the PMA is demonstrated to originate from the interface hybridizations and is sensitive to electron filling[42–45]. At the same time, the coercivity has been found being linked to the changes of the magnetic anisotropy[46,47] in the case of either the single-domain or the nucleation and domain wall propagation switching model. It is reported that the hybridization between Pt 5d and Co 3d at the interface in Co/Pt multilayers enhances the orbital

https://doi.org/10.1038/s41467-025-59689-z

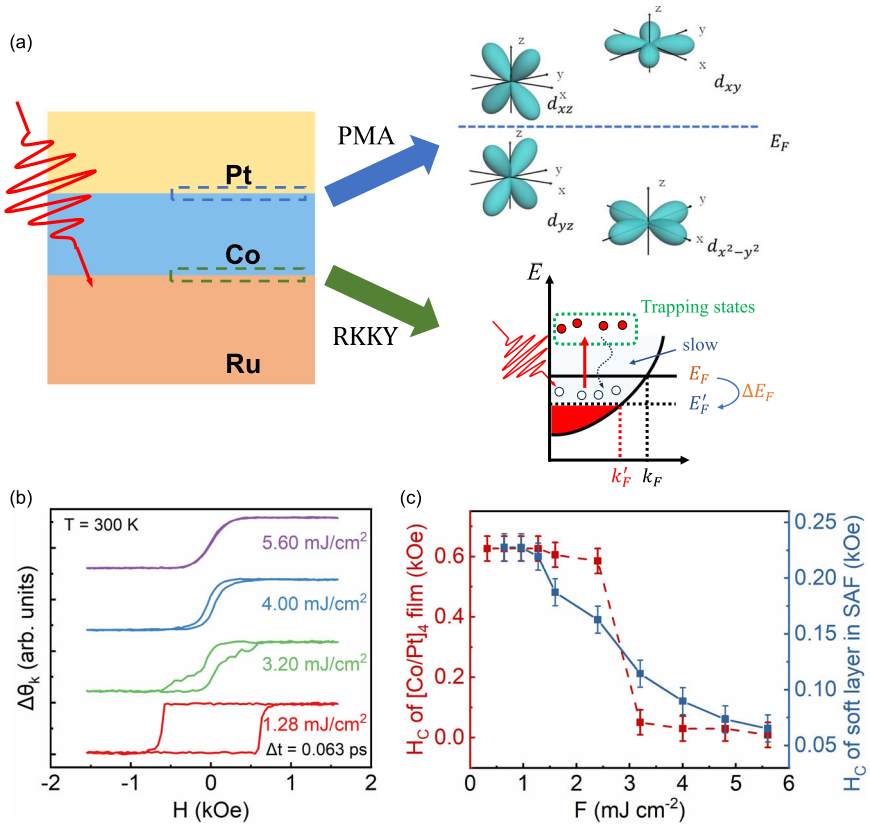

Fig. 4 | Schematic diagram of optical control of the PMA and the RKKY. **a** Diagram of how fs-laser excitations modulate the RKKY coupling and the PMA in a SAF system. Upon fs excitations, the pump photon energy (1.55 eV) excites electrons in Ru (indicated by the red vertical arrow) from occupied states below the Fermi level E_F to unoccupied trapping states above E_F, resulting a down-shift of the Fermi level from E_F to E_F'. Considering the parabolic band dispersion at the Ru interface, a downshift of E_F can result in a decrease in the RKKY coupling. Meanwhile, at the Co/Pt interface such a ΔE_F shift will cause electron redistributions between d_{xz} and d_{yz} orbitals due to a smaller energy gap, thus causing a concomitant reduction of the PMA. **b** Transient hysteresis loops recorded at 0.063 ps under different pump fluences for a thin $[Co/Pt]_4$ film. **c** Extracted H_C values from the $[Co/Pt]_4$ thin film and from the soft layer in the SAF sample as a function of pump fluence. Here, the $[Co/Pt]_4$ stack is inserted in a sample structure of Ta(4)/Pt(4)/[Pt(0.6)/Co(0.6)]$_4$/Ta(2) without the RKKY coupling. Error bars indicate the uncertainty in determining the displayed value from the experimentally measured data.

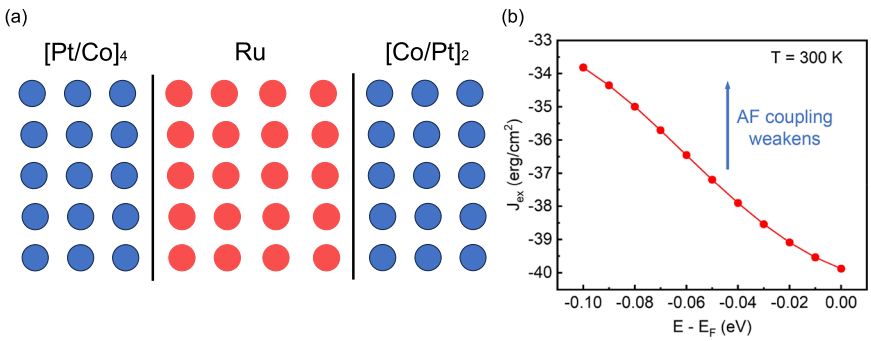

Fig. 5 | Influence of Fermi level shift ($E - E_F$) on AF coupling J_{ex} by First-principle calculations. **a** The sketched lattice interface of the SAF structure for calculations. **b** The calculated AF coupling J_{ex} as a function of the shift of Fermi level.

magnetic moment, thus the PMA due to spin orbital interaction (SOC)[42]. In specific, the SOC matrix elements with the same spin $\langle d_{xy}|H_{SO}|d_{x^2-y^2}\rangle$ and $\langle d_{xz}|H_{SO}|d_{yz}\rangle$ contributes to PMA[42,44]. d_{xz} and d_{yz} orbitals are split by SOC with an energy gap of 70 meV. While d_{xy} and $d_{x^2-y^2}$ are located by the crystal field with an energy separation much larger than 70 meV[45]. Thus, electron occupations between d_{xz} and d_{yz} orbitals at the Co/Pt interface are more easily to be modulated by perturbations such as optical excitations.

As depicted in the right-upper part of Fig. 4a, ΔE_F occurs simultaneously at the Pt/Co interface (also at the Co/Ru interface as mentioned above), leading to electron redistributions therein, for example, between d_{xz} and d_{yz} orbitals. This can diminish the PMA, similar to previous reports of E-field control on PMA[29,30,48]. In the absence of the interlayer interaction for a $[Co/Pt]_4$ thin film (Fig. 4b), its H_C (red squares in Fig. 4c) shows a step-like decrease as a function of F, while the H_C in the SAF (blue squares in Fig. 4c) declines continuously. This contrast suggests that the deviations of H_C in a SAF structure is caused by H_{ex}. Therefore, when H_{ex} is modulated by fs laser excitations due to ΔE_F, H_C is changed consecutively.

In our experiments, the RKKY field H_{ex} shows a drop by 4.9%. This corresponds to an E_F shift of ~35 meV according to our theory calculations in Fig. 5b. Such a shift is large enough to cause the electron

redistributions among d_{xz} and d_{yz} orbitals with a gap of 70 meV, and thus modifying PMA.

The above proposed explanation involves a photoexcitation process, which means that changing the pump excitation may give rise to different modulations on both H_{ex} and H_C. This is verified by exchanging the pump and probe wavelengths, namely, exciting the sample with a photon energy of 3.1 eV while probing the dynamics with a photon energy of 1.55 eV. As shown in the Fig. S5 (Supplementary Note 5), H_{up} of the transient minor loops excited by the 400 nm laser show an obvious decrease at $F = 0.48$ mJ/cm^2, and remains almost stable after $F = 0.80$ mJ/cm^2. For the 800 nm excitations in Fig. 2, variations of H_{up} actually occur after $F = 1$ mJ/cm^2. Such an efficient excitation by a 400 nm pulse is supported by the measured optical reflectivity spectrum. As shown in Fig. S6c, SAF reflectivity at 800 nm is larger than that at 400 nm, showing larger absorption at 400 nm. More efficient excitations by 400 nm are likely due to the generated nonthermal electrons at higher energy levels. If the absorbed-photon amounts play a role, the transient MOKE loops at higher pump fluence pumped by 800 nm would be similar to the MOKE loops pumped by 400 nm laser at a low fluence (see also Supplementary Note 5). However, the shapes of transient loops excited by 800 nm and 400 nm are clearly different. Thus, nonthermal electrons contributions to the efficient excitations are preferred.

Here, the optically modulated RKKY and PMA assisted by trapping states have been found to affect the switching process of SAF magnetization (Fig. S7) and magnetization precession dynamics (Fig. S8), which may have potential ultrafast spintronic applications. Recent research on a PN-Si/CoFe/Cu/CoFe sample demonstrates that light illumination induces a switch between FM and AFM states[49], where there is an exchange of photoexcited electrons or carriers between the SAF layer and the substrate. In our current study, the naturally oxidized SiO_2 layer on a Si substrate prevented the generation and propagation of any photoexcited electrons or carriers. With a combination of a SAF structure and a clean semiconductor surface, the RKKY and PMA may be optically modulated more profoundly. However, such a study is beyond the scope of this work.

In summary, our investigation of the transient hysteresis loops in a synthetic antiferromagnetic structure shows optical modulations on the RKKY interaction and the MAE by a femtosecond laser pulse. By increasing the pump fluence, simultaneous reductions of both the H_{ex} and the H_C are observed. The results are explained in terms of changes in the electronic DOS and orbital occupancy at the Co/Ru and Pt/Co interfaces. The fs-pulse excitation induces a downshift of the Fermi level E_F within the Ru layer, subsequently reducing the Fermi wave vector k_F and then resulting in a continuous decline of the RKKY coupling. Meanwhile, the Fermi level shift lunches subtle electron transfer at the Pt/Co interface between d_{xz} and d_{yz} orbitals, leading to a decrease in the PMA. As expected from our proposed model, different pump excitation process (400 nm vs 800 nm) is shown to have an impact on the modulations. Our results achieve, for the first time, optical control of the RKKY coupling and the PMA by a femtosecond laser pulse and provide fundamental understandings on this. The findings are expected to play an important role in the energy-efficient magnetization switching.

Methods

Sample preparation and VSM measurement

The sample was grown via high-vacuum magnetron sputtering on Si substrates with a native oxide. The base pressure is maintained at less than 1×10^{-7} Pa. The static magnetic properties were measured by a vibrating sample magnetometer (VSM) at room temperature.

Time-resolved MOKE/reflectivity measurements

The magnetization dynamics were investigated using the Time-Resolved Magneto-Optical Kerr Effect (TR-MOKE) technique, employing a pulsed Ti:sapphire regenerative amplifier with a central wavelength of 800 nm, a pulse duration of approximately 50 fs, and a repetition rate of 1 kHz. Dynamic behaviors were induced by an intense pump pulse laser at 800 nm, while the transient MOKE signals were detected by a time-delayed probe beam at 400 nm with a much lower intensity. Another beam splitter was placed in the probe beam path, before it was reflected from the sample, to obtain the reference beam and probe pulses for TR-reflectivity measurements. The pump beam was incident on the sample with a 400 μm diameter spot size, while the probe beam was angled approximately 4° away from the normal direction of the film plane, with a spot size of 250 μm in diameter. The external magnetic field was applied perpendicular to the sample surface. In this configuration, the Kerr rotation is sensitive only to changes in the out-of-plane magnetization component. To precisely determine the time zero, please refer to Supplementary Note 3 in the Supporting Information.

Data availability

All data needed to evaluate the conclusions in the paper are present in the paper and/or the Supplementary Information. The data used for the presented analysis are publicly available under https://doi.org/10.5281/zenodo.15285414. Source data are provided with this paper.

References

1. Železný, J. et al. Relativistic N'eel-order fields induced by electrical current in antiferromagnets. *Phys. Rev. Lett.* **113**, 157201 (2014).
2. Wadley, P. et al. Electrical switching of an antiferromagnet. *Science* **351**, 587–590 (2016).
3. Chen, B. B. et al. All-oxide-based synthetic antiferromagnets exhibiting layer-resolved magnetization reversal. *Science* **357**, 191–194 (2017).
4. Nishitani, J. et al. Terahertz radiation from coherent antiferromagnetic magnons excited by femtosecond laser pulses. *Appl. Phys. Lett.* **96**, 221906 (2010).
5. Kampfrath, T. et al. Coherent terahertz control of antiferromagnetic spin waves. *Nat. Photonics* **5**, 31–34 (2011).
6. Jin, Z. et al. Single-pulse terahertz coherent control of spin resonance in the canted antiferromagnet $YFeO_3$, mediated by dielectric anisotropy. *Phys. Rev. B* **87**, 094422 (2013).
7. Nishitani, J. et al. Coherent control of terahertz radiation from antiferromagnetic magnons in NiO excited by optical laser pulses. *Phys. Rev. B* **85**, 174439 (2012).
8. Jungwirth, T. et al. Antiferromagnetic spintronics. *Nat. Nanotechnol.* **11**, 231–241 (2016).
9. Marti, X. et al. Room-temperature antiferromagnetic memory resistor. *Nat. Mater.* **13**, 367–374 (2014).
10. Stiles, M. D. Interlayer exchange coupling. *J. Magn. Magn. Mater.* **200**, 322–337 (1999).
11. Parkin, S. S. P. Systematic variation of the strength and oscillation period of indirect magnetic exchange coupling through the 3d, 4d, and 5d transition metals. *Phys. Rev. Lett.* **67**, 3598–3601 (1991).
12. Yang, Q. et al. Ionic liquid gating control of RKKY interaction in FeCoB/Ru/FeCoB and $(Pt/Co)_2/Ru/(Co/Pt)_2$ multilayers. *Nat. Commun.* **9**, 991 (2018).
13. Ameziane, M. et al. Electric field control of RKKY coupling through solid-state ionics. *Appl. Phys. Lett.* **122**, 232401 (2023).
14. Kossak, A. E. et al. Voltage control of magnetic order in RKKY coupled multilayers. *Sci. Adv.* **9**, eadd0548 (2023).
15. Fechner, M. et al. Switching magnetization by 180° with an electric field. *Phys. Rev. Lett.* **108**, 197206 (2012).
16. Leon, A. O. et al. Manipulation of the RKKY exchange by voltages. *Phys. Rev. B* **100**, 014403 (2019).
17. You, C. Y. et al. Prediction of switching rotation of the magnetization direction with applied voltage in a controllable interlayer exchange coupled system. *J. Magn. Magn. Mater.* **195**, 488–500 (1999).

18. You, C. Y. et al. Voltage controlled spintronic devices for logic applications. *J. Appl. Phys.* **87**, 5215–5217 (2000).
19. Diez, L. H. et al. Magneto-ionic and electrostatic gating of magnetism: Phenomena and devices. *Appl. Phys. Lett.* **123**, 130401 (2023).
20. Fan, Y. et al. Exchange bias of the interface spin system at the Fe/MgO interface. *Nat. Nanotechnol.* **8**, 438–444 (2013).
21. Ju, G. P. et al. Ultrafast time resolved photoinduced magnetization rotation in a ferromagnetic/antiferromagnetic exchange coupled system. *Phys. Rev. Lett.* **82**, 3705–3708 (1999).
22. Liu, B. et al. Light-tunable ferromagnetism in atomically thin Fe_3GeTe_2 driven by femtosecond laser pulse. *Phys. Rev. Lett.* **125**, 267205 (2020).
23. Wang, J. et al. Ultrafast enhancement of ferromagnetism via photoexcited holes in GaMnAs. *Phys. Rev. Lett.* **98**, 217401 (2007).
24. Matsubara, M. et al. Ultrafast optical tuning of ferromagnetism via the carrier density. *Nat. Commun.* **6**, 6724 (2015).
25. Fernández-Rossier, J. et al. Coherently photoinduced ferromagnetism in diluted magnetic semiconductors. *Phys. Rev. Lett.* **93**, 127201 (2004).
26. Ke, M. et al. Nonequilibrium RKKY interaction in irradiated graphene. *Phys. Rev. Res.* **2**, 033228 (2020).
27. Gorchon, J. et al. Single shot ultrafast all optical magnetization switching of ferromagnetic Co/Pt multilayers. *Appl. Phys. Lett.* **111**, 042401 (2017).
28. Chatterjee, J. et al. RKKY exchange bias mediated ultrafast all-optical switching of a ferromagnet. *Adv. Funct. Mater.* **32**, 2107490 (2022).
29. Weisheit, M. et al. Electric field-induced modification of magnetism in thin-film ferromagnets. *Science* **315**, 349–351 (2007).
30. Maruyama, T. et al. Large voltage-induced magnetic anisotropy change in a few atomic layers of iron. *Nat. Nanotechnol.* **4**, 158–161 (2009).
31. Quessab, Y. et al. Helicity-dependent all-optical domain wall motion in ferromagnetic thin films. *Phys. Rev. B* **97**, 054419 (2018).
32. Shim, J.-H. et al. Ultrafast giant magnetic cooling effect in ferromagnetic Co/Pt multilayers. *Nat. Commun.* **8**, 796 (2017).
33. Shim, J.-H. et al. Ultrafast dynamics of exchange stiffness in Co/Pt multilayer. *Commun. Phys.* **3**, 74 (2020).
34. Shim, J.-H. et al. Role of non-thermal electrons in ultrafast spin dynamics of ferromagnetic multilayer. *Sci. Rep.* **10**, 6355 (2020).
35. Liu, B. et al. Microscopic insights to spin transport–driven ultrafast magnetization dynamics in a Gd/Fe bilayer. *Sci. Adv.* **9**, eade0286 (2023).
36. Kübler, J. *Theory of Itinerant Electron Magnetism*. Vol. 106, 277–280 (Oxford University Press, 2017).
37. Ishioka, K. et al. Intrinsic coherent acoustic phonons in the indirect band gap semiconductors Si and GaP. *Phys. Rev. B* **95**, 035205 (2017).
38. Temnov, V. V. et al. Femtosecond nonlinear ultrasonics in gold probed with ultrashort surface plasmons. *Nat. Commun.* **4**, 1468 (2013).
39. Liu, P. et al. Ultrafast optical control of surface and bulk magnetism in magnetic topological insulator/antiferromagnet heterostructure. *Sci. Rep.* **12**, 12117 (2022).
40. Wang, S. et al. Modulations of interlayer exchange coupling through ultrathin MgO-based magnetic tunnel junctions: First-principles study. *Phys. Rev. B* **96**, 024443 (2017).
41. Li, C. et al. Sunlight control of ferromagnetic damping in photovoltaic/ferromagnetic heterostructures. *Adv. Funct. Mater.* **32**, 2111652 (2022).
42. Nakajima, N. et al. Perpendicular magnetic anisotropy caused by interfacial hybridization via enhanced orbital moment in Co/Pt multilayers: magnetic circular X-ray dichroism study. *Phys. Rev. Lett.* **81**, 5229–5232 (1998).
43. Kyuno, K. et al. First-principles calculation of the magnetic anisotropy energies of Ag/Fe(001) and Au/Fe(001) multilayers. *J. Phys. Soc. Jpn.* **65**, 1334–1339 (1996).
44. Bruno, P. Tight-binding approach to the orbital magnetic moment and magnetocrystalline anisotropy of transition-metal monolayers. *Phys. Rev. B* **39**, 865–868 (1989).
45. Wang, D. et al. Magnetocrystalline anisotropy of Co-Pd interfaces. *Phys. Rev. B* **48**, 15886–15892 (1993).
46. Zhao, X. et al. Enhancing domain wall velocity through interface intermixing in W-CoFeB-MgO films with perpendicular anisotropy. *Appl. Phys. Lett.* **115**, 122404 (2019).
47. Devolder, T. et al. Magnetic properties of He^+-irradiated Pt/Co/Pt ultrathin films. *Phys. Rev. B* **64**, 064415 (2001).
48. Niranjan, M. K. et al. Electric field effect on magnetization at the Fe/MgO(001) interface. *Appl. Phys. Lett.* **96**, 222504 (2010).
49. Du, Y. et al. Deterministic magnetization reversal in synthetic antiferromagnets using natural light. *Small* **19**, 2302884 (2023).

Acknowledgements

This work is supported by the National Key Research and Development Program of China (Grant Nos. 2024YFA1408801, 2023YFA1406601), the National Natural Science Foundation of China (Grant Nos. 12474118, 62427901), and the Fundamental Research Funds for the Central Universities (2024300355). This work is also partly supported by the Natural Science Foundation of Jiangsu Province of China (Grant Nos. BK20200307, BK20192006, BK20180056, BK20211144), the National Natural Science Foundation of China (Grant Nos. 12104216, 61427812, 11774160, 61805116, 12241403, T2394473, T2394470, 12374112, 11734004). The authors thank Xiang Peng and Wangheng Pan for their contributions in optical reflectivity measurements.

Author contributions

B.L. and Y.X. conceived the project. Z.L. prepared the samples and M.M. performed the measurements with the assistance of T.L., X.R., X.L. and J.D., M.M., B.L. and J.W. performed data analysis. L.W. and K.X. performed first-principle calculations. Z.H. and F.W. performed the optical reflectivity measurements. M.M., B.L. and Y.X. wrote the manuscript. All the authors discussed the results and commented on the manuscript. The study was supervised by Y.X., B.L.

Competing interests

The authors declare no competing interests.

Additional information

Supplementary information The online version contains supplementary material available at https://doi.org/10.1038/s41467-025-59689-z.

Correspondence and requests for materials should be addressed to Jing Wu, Bo Liu or Yongbing Xu.

Peer review information *Nature Communications* thanks Jyotirmoy Chatterjee, and the other, anonymous, reviewer(s) for their contribution to the peer review of this work. A peer review file is available.